A simple polyol-free synthesis route to Gd 2O 3 nanoparticles for MRI applications: An experimental and theoretical study

ARTICLE *in* JOURNAL OF NANOPARTICLE RESEARCH · AUGUST 2012

Impact Factor: 2.18 · DOI: 10.1007/s11051-012-1006-2

J Nanopart Res (2012) 14:1006
DOI 10.1007/s11051-012-1006-2

RESEARCH PAPER

A simple polyol-free synthesis route to Gd_2O_3 nanoparticles for MRI applications: an experimental and theoretical study

Maria Ahrén · Linnéa Selegård · Fredrik Söderlind · Mathieu Linares · Joanna Kauczor · Patrick Norman · Per-Olov Käll · Kajsa Uvdal

Received: 24 February 2012 / Accepted: 18 June 2012

Abstract Chelated gadolinium ions, e.g., Gd-DTPA, are today used clinically as contrast agents for magnetic resonance imaging (MRI). An attractive alternative contrast agent is composed of gadolinium oxide nanoparticles as they have shown to provide enhanced contrast and, in principle, more straightforward molecular capping possibilities. In this study, we report a new, simple, and polyol-free way of synthesizing 4–5-nm-sized Gd_2O_3 nanoparticles at room temperature, with high stability and water solubility. The nanoparticles induce high-proton relaxivity compared to Gd-DTPA showing r_1 and r_2 values almost as high as those for free Gd^{3+} ions in water. The Gd_2O_3 nanoparticles are capped with acetate and carbonate groups, as shown with infrared spectroscopy, near-edge X-ray absorption spectroscopy, X-ray photoelectron spectroscopy and combined thermogravimetric and mass spectroscopy analysis. Interpretation of infrared spectroscopy data is corroborated by extensive quantum chemical calculations. This nanomaterial is easily prepared and has promising properties to function as a core in a future contrast agent for MRI.

Keywords Gadolinium oxide · Synthesis · Relaxivity · XPS · IR · Toxicity

Electronic supplementary material The online version of this article (doi:10.1007/s11051-012-1006-2) contains supplementary material, which is available to authorized users.

M. Ahrén · L. Selegård · K. Uvdal (✉)
Division of Molecular Surface Physics and Nanoscience, Department of Physics, Chemistry and Biology (IFM), Linköping University, 581 83 Linköping, Sweden
e-mail: kajsa@ifm.liu.se

F. Söderlind
Division of Nanostructured Materials, Department of Physics, Chemistry and Biology (IFM), Linköping University, 581 83 Linköping, Sweden

M. Linares · J. Kauczor · P. Norman
Division of Computational Physics, Department of Physics, Chemistry and Biology (IFM), Linköping University, 581 83 Linköping, Sweden

P.-O. Käll
Division of Chemistry, Department of Physics, Chemistry and Biology (IFM), Linköping University, 581 83 Linköping, Sweden

Introduction

Over the last decade, considerable efforts have been made to increase the contrast in magnetic resonance imaging (MRI). So far, two main groups of contrast agents have been in focus for clinical use; nanosized superparamagnetic iron oxide particles delivering negative contrast and paramagnetic agents based on Gd(III) chelates delivering positive contrast (Geraldes and Laurent 2009). Today, however, the interest for negative contrasts has been reduced, due to the fact that contrast agents such as iron oxide particles lower the signal strength in MRI and deliver darker images. Thus, Gd-based metal ion complexes completely

Published online: 10 July 2012

dominate the market. Gd^{3+} possesses, due to its electron configuration with seven unpaired *f*-electrons, a large magnetic moment ($\sim$7.9 BM). The combination of the large magnetic moment and the symmetry of the electronic state induce very high-longitudinal relaxivities of nearby protons (Caravan et al. 1999; Lauffer 1987). Researchers around the world now strive to develop a new generation of Gd-based agents with further improved relaxation properties to enhance the MRI sensitivity and achieve improved image contrast compared to what is possible today. Another strongly desired goal is to equip (functionalize) these new contrast agents for tissue targeting purposes and/or to enable drug delivery.

In all kinds of gadolinium-based contrast agents, the presence of free gadolinium ions has to be avoided due to the cytotoxicity. The conventional way of producing a gadolinium-based contrast agent is to form a chelate, i.e., stabilizing the metal ion using a chelating agent (for example, DTPA or DOTA) but recently several other strategies have been proposed. Among these, metallofullerenes where the Gd ions are encapsulated in a fullerene cage (Toth et al. 2005; Shu et al. 2009; Zhang et al. 2010a; Bolskar et al. 2003), metal–organic frameworks (MOFs) (Rowe et al. 2009b; Rieter et al. 2006; Rowe et al. 2009a), and nanoscale coordination polymers (NCP) (Zhang et al. 2010b) can be mentioned. The synthesis of the latter compounds, however, is typically quite complicated normally involving several steps. A main limitation of organic systems like MOFs and metallofullerenes is their large size (often >100 nm), since large molecular species are usually quickly recognized by phagocytes and removed by the reticulo-endothelial system (RES) (Skotland et al. 2010; Alexis et al. 2008). The size of a nanoparticle contrast agent is thus a critical parameter as is also its chemical stability.

Concerning Gd-based contrast agents, clearance through the kidneys is required in order to avoid accumulation in the body. The cutoff for renal excretion of nanoparticles is below 10 nm, and, in general, renal excretion increases with decreasing particle size (Skotland et al. 2010). In addition to the benefit of renal clearance, there are other advantages in working with very small particles as MRI contrast enhancers, such as prolonged examination time as a consequence of a prolonged circulation time. Small-sized systems also have an extended field of application, since direct particle–cellular and particle–molecular interactions become feasible (Na and Hyeon 2009). While the MRI technique has an inherently low sensitivity, it is a main goal to increase the number of Gd ions available to water molecules per contrast agent unit. In MOFs, the amount of Gd ions is severely restricted by the organic framework, and, in metallofullerenes, the Gd ions are encased behind a shield of organic molecules; in both the cases, the number of Gd ions incorporated strongly influences the size of the system.

The most efficient way to collect a large number of Gd ions within a small volume is to use nanocrystals of, e.g., gadolinium oxide (Gd_2O_3) (Bridot et al. 2007; Fortin et al. 2007; McDonald and Watkin 2006; Park et al. 2009; Söderlind et al. 2005; Petoral Jr et al. 2009; Kim et al. 2010), gadolinium fluoride (GdF_3) (Evanics et al. 2006; Chaput et al. 2011), or gadolinium phosphate ($GdPO_4$) (Hifumi et al. 2006; Yan et al. 2010; Lai et al. 2008). The crystals preferably are kept small enough to give a large surface to bulk ratio and thereby an efficient interaction between Gd^{3+} and water molecules; i.e., a high-water exchange. Small or ultrasmall Gd_2O_3 nanoparticles synthesized according to the polyol route have been extensively studied, by our group and others (Bridot et al. 2007; Fortin et al. 2007; McDonald and Watkin 2006; Park et al. 2009; Petoral Jr et al. 2009; Söderlind et al. 2005). The yield of the polyol synthesis is rather low though, and a severe drawback is the necessity to apply lengthy dialysis times to purify the nanoparticle solutions from free Gd^{3+}. Moreover, as-synthesized polyol-prepared nanoparticles are usually dispersed in diethylene glycol (DEG), a toxic chemical which is known to induce renal failure in poisoning accidents, thus not suitable for oral intake or intravenous injection (Peng et al. 2009; Schep et al. 2009). Exchanging DEG on the nanoparticle surface to a biocompatible and/or targeting capping layer and transferring the nanoparticle dispersions to water, without disrupting the nanoparticles, are tasks that have shown to be less controllable as well as time-consuming. Another synthesis method, which is based on ethylene glycol (EG) instead of DEG, performed at lower temperature and during shorter time has been presented lately (Rahman et al. 2011). Gd_2O_3 nanoparticles have also been synthesized by the combustion method yielding a highly crystalline nanoparticle powder (Söderlind et al. 2005). Aggregation is, however, severe for such as-synthesized Gd_2O_3 nanoparticles, and the solubility

in water is extremely low, making MRI studies impossible.

In this article, we report a new way of synthesizing very small Gd_2O_3 nanoparticles. The synthesis is free from a polyol solvent (e.g., DEG) performed at room temperature, and the nanocrystalline powder after washing and drying shows high solubility and stability in water solution. This study of non-functionalized Gd_2O_3 nanoparticles is an initial step toward biocompatible and directed nanoparticles. The main focus is on a material that in the nearby future will be the core of an actively functionalized nanomaterial for MRI contrast enhancement. The material was characterized with X-ray powder diffraction (XRD), transmission electron microscopy (TEM), dynamic light scattering (DLS), Fourier transform infrared spectroscopy (FT-IR), near-edge X-ray absorption fine structure spectroscopy (NEXAFS), X-ray photoelectron spectroscopy (XPS), and thermogravimetry combined with mass spectroscopy (TG-MS). The longitudinal and transverse magnetic resonance relaxivities (r_1 and r_2) were measured with an NMR analyzer. The experimental results are supported by theoretical modeling studies. Theoretical IR spectra of three different Gd acetate complexes are presented as well as calculated NEXAFS spectra of one of the Gd acetate complexes and an isolated acetate group. These calculations were performed to elucidate the molecular capping of the synthesized particles.

Experimental details

Chemicals

All chemicals were used as received: gadolinium(III) acetate hydrate (Sigma-Aldrich, 99.9 %), tetramethylammonium hydroxide (Sigma-Aldrich, >97 %), ethyl acetate (Fisher Scientific, 99.99 %), dimethyl sulfoxide (Merck, 99.9 %), ammonium acetate (Merck, >96 %), ethanol (Kemetyl, 99.5 %). For preparation of water-based solutions, Milli-Q water ($\rho > 18.2$ MΩ) was used. A commercial gadolinium oxide nanopowder (Aldrich, <100 nm, 99.8 %) was used as a reference.

Preparation of Gd_2O_3 nanoparticles

The preparation of Gd_2O_3 nanoparticles was based on a method previously used for producing nanocrystalline ZnO (Schwartz et al. 2003). As Zn^{2+} is divalent and Gd^{3+} is trivalent, the molar amount of gadolinium(III) acetate was reduced in order to keep the same over-all charge concentration in the Gd_2O_3 synthesis as in the ZnO synthesis. The synthesis was performed at room temperature by dropwise adding 10 ml of 0.55 M tetramethylammonium hydroxide (TMAH) in ethanol to 30 ml of 0.067 M gadolinium(III) acetate in dimethyl sulfoxide under constant stirring. Precipitation was noticed during the dropwise addition of TMAH. After addition of TMAH, stirring was continued at room temperature for 1 h. Ethyl acetate was added, and the mixture was centrifuge washed (3,500 rpm) at least three times with ethyl acetate before it was diluted in deionized water. A total amount of 0.28 g ammonium acetate was added to one whole batch to increase the water solubility. Powder samples were air dried. The yield of the sample is dependent on the washing procedure. The gadolinium content after three times of centrifuge washing with ethyl acetate is roughly 60–65 % of the initial amount added in the synthesis.

Instrumentation

X-ray diffraction

X-ray diffraction (XRD) measurements were carried out with a Philips XRD powder diffractometer using Cu Kα radiation ($\lambda = 1.5418$ Å, 40 kV, 40 mA). The 2θ step-size was 0.025° and the time per step 4 s. Air-dried powder samples were used in the preparation.

High-resolution transmission electron microscopy

High-resolution transmission electron microscopy (HR-TEM) measurements were performed on a FEI Tecnai G^2 electron microscope operated at 200 kV. Sample preparation was done by letting 1–2 drops of Gd_2O_3 in water dry on an amorphous carbon-covered copper grid.

Dynamic light scattering

Dynamic light scattering (DLS) measurements were carried out on an ALV/DLS/SLS-5022F system from ALV-GmbH, Langen, Germany, using a HeNe laser at 632.8 nm with 22 mW output power. Prior to the measurements, the samples were temperature stabilized in a thermostat bath at 22.1 °C for at least 10 min. The scattering angle was 90°. 15 Gd_2O_3 samples dispersed

in MilliQ water were studied in DLS, and the long-term stability of the suspensions were studied by repeated measurements during a period of 6 weeks.

ζ Potential

ζ potential measurements were carried out on a Model Zetasizer Nano ζ-Potential Analyzer (Malvern Instruments, UK). Temperature was 25 °C. The as-synthesized and three times ethyl acetate centrifuge washed nanoparticle suspension was highly diluted with deionized water prior to measurement.

Infrared spectroscopy

Transmission IR studies were done on a Bruker Vertex 70 FT-IR instrument using pressed pellets of KBr. Measurements were performed in the range 400–4,800 cm^{-1}, and ~300 mg KBr and 1 mg sample powder were used in the preparation of each pellet.

X-ray photoelectron spectroscopy

X-ray photoelectron spectroscopy (XPS) measurements were performed at the MAX II synchrotron storage ring at MAX-Lab in Lund, Sweden. The beamline used was D1011. The photon energy was optimized for each atomic element according to: survey spectra and Gd 3d spectra at 1,300 eV, C 1s spectra at 385 eV, and O 1s spectra at 650 eV. The binding energy scales of the spectra were aligned through the C 1s peak (285 eV). Peak positions were found to shift nonlinearly upon different photon energies, most likely because of an imperfect linearity of the monochromator, and the final alignment was based also on elemental peak position separations in a survey scan with photon energy 1,300 eV. Si (100) substrates for XPS measurements were cleaned in a 5:1:1 mixture of MilliQ water, 25 % hydrogen peroxide and 30 % ammonia for 10 min at 80 °C and rinsed in MilliQ water. Drops of sample solution was added to the surfaces and dried with N_2.

Near-edge X-ray absorption fine structure spectroscopy

As for XPS, NEXAFS measurements were performed at the synchrotron storage ring MAX II at MAX-Lab in Lund, Sweden. The beamline used was D1011, and samples were prepared as for XPS. Retardation voltage was set to −40, −150, −400, and −800 V for Gd 4d, C 1s, O 1s, and Gd 3d, respectively.

Thermogravimetry and mass spectroscopy analysis

Thermal analysis was performed using a Netzsch STA 449C Jupiter instrument, and in situ gas analysis was conducted simultaneously using a mass spectrometer (Netzsch: QMS 403C Aëolos) through a heated transfer capillary. Approximately 10 mg of air-dried Gd_2O_3 nanoparticle powder was placed in a sintered Al_2O_3 crucible at room temperature. The temperature was increased to 1,100 °C at a rate of 10 °C/min. The temperature was held at 200 °C for 30 min. The studies were performed under He flow (100 mL/min).

Relaxation measurement

The relaxation measurements were performed on a Bruker minispec mq60 NMR analyzer at 40 °C using a magnetic field of 1.41 T. Samples were diluted in MilliQ water to different Gd concentrations in the approximate range 0–2 mM prior to the measurement. The absolute concentrations were determined afterward by ICP-MS at ALS Scandinavia AB (Sweden).

Computational details

IR spectroscopy modeling

Geometry optimizations and IR frequency calculations were carried out with the Gaussian program (Frisch 2003) with the use of density functional theory (DFT) in conjunction with the B3LYP exchange correlation functional (Becke 1993) and Dunning's cc-pVTZ family of basis sets for light elements (Dunning 1989) and the large core Stuttgart effective potential (SDD) for gadolinium (Dolg et al. 1989). The IR spectra were obtained in the harmonic force field approximation based on analytic molecular Hessians. The presented frequencies have been scaled by a factor of 0.97.

Geometries considered in IR spectroscopy modeling

From the literature, we considered three complexes with a coordination number of nine for the gadolinium atom. All three complexes are shown in Fig. 1. In the

first complex $[Gd(OAc)_4(H_2O)_2]^-$ (Fig. 1a), the gadolinium atom is coordinated to three bidentate acetate ligands, two water molecules and an oxygen atom from a bridging acetate ligand (Favas et al. 1980). The second complex, which presents a center of inversion, is the dimer form of the first complex: $[Gd(OAc)_3(H_2O)_2]_2$ (Fig. 1b) (Hatscher and Urland 2003). For each gadolinium atom, the coordination scheme is the same as for the monomer. The last structure considered is composed of two gadolinium atoms, eight acetate groups and no water $[Gd_2(OAc)_8]^{2-}$ (Fig. 1c) (Smith and Ryan 1992).

NEXAFS modeling

We calculated the NEXAFS spectra of the dimer (Fig. 1b) and the isolated acetate, using the geometry optimized at the B3LYP/cc-pVTZ level of theory. The linear absorption cross-section is proportional to the imaginary part of the electric-dipole polarizability in accordance with the expression (Boyd 2003)

$$\sigma(\omega) = \frac{4\pi\omega}{c}\mathrm{Im}[\bar{\alpha}(\omega)], \quad (1)$$

where c is the speed of light and ω is the angular frequency of the incident radiation. The calculation of the NEXAFS spectrum has been performed with the use of a locally modified version of the DALTON program (Jensen et al. 2005), employing the Coulomb attenuated method B3LYP (CAM-B3LYP) exchange–correlation functional (Yanai et al. 2004) with a set of parameters that guarantees a correct asymptotic limit of the Coulomb hole–electron interaction (Ekström and Norman 2006) ($\alpha = 0.19$, $\beta = 0.81$, and $\mu = 0.33$). The basis set used in this calculation is aug-cc-pVDZ for light elements and the large core Stuttgart effective potential for gadolinium (Dolg et al. 1989). The polarizability is identified from the damped linear response function (Norman et al. 2001, 2005), using a very efficient recently implemented solver (Kauczor et al. 2011), and the present calculations are carried out with a damping parameter that equals 1,000 cm^{-1}. From a technical point of view, we note that the solving of the damped linear response equations is enabled by the implementation of a linear response solver in accordance with the symmetrized trial vector algorithm presented by Kauczor et al. (2011).

Results and discussion

In this article, a new synthesizing procedure to obtain Gd_2O_3 nanoparticles to be used for MRI contrast enhancement is presented. The synthesis is DEG free, fast, and performed at room temperature. The characterization is focused on crystallinity, particle size and size distribution, chemical composition, and relaxivity properties.

Crystallinity, size, and size distribution

The XRD pattern of Gd_2O_3 nanoparticle powder is presented in Fig. 2b together with a reference diffractogram of a Gd_2O_3 bulk powder in Fig. 2a. The Gd_2O_3 nanopowder displays one broad peak centered at $2\theta \approx 29°$, which is identified as the 222 reflection of cubic Gd_2O_3. The extensive peak broadening and low intensity are most likely due to the small nanoparticle size (Weller 1994). In general, the atomic scattering factor is high for atoms with high-atomic number (Gd: $Z = 64$), but the low-peak intensities observed for the

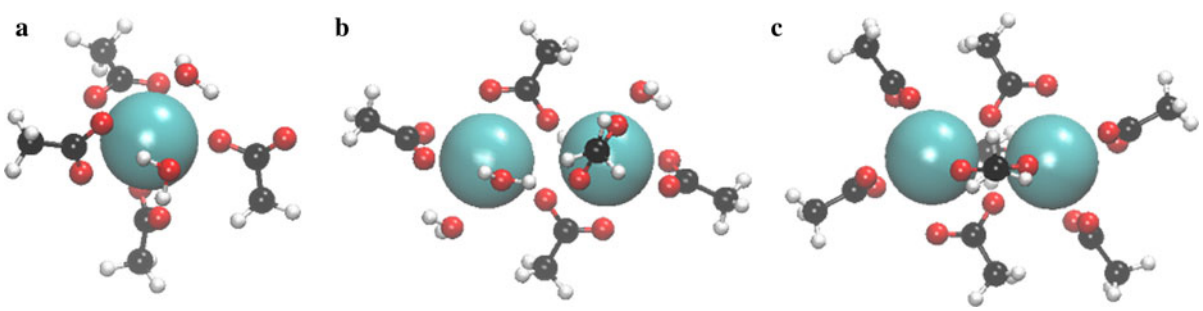

Fig. 1 The three different gadolinium acetate complexes considered in the theoretical IR calculations: **a** $[Gd(OAc)_4(H_2O)_2]^-$, **b** $[Gd(OAc)_3(H_2O)_2]_2$, and **c** $[Gd_2(OAc)_8]^{2-}$

Gd sample in Fig. 2b is probably also a consequence of gadolinium fluorescence (Gustafsson et al. 2011).

Transmission electron microscopy (TEM) was used to characterize the material concerning the crystal structure, shape, size, and size distribution of the nanoparticles. A representative HR-TEM image of a freshly synthesized Gd_2O_3 nanoparticle material is shown to the left in Fig. 3 together with the corresponding FFT pattern. The TEM image shows the projection of more or less spherically shaped crystallites with an estimated size of 4–5 nm. The FFT diffraction pattern shows the expected spots representing the (222), (400), (440), and the (622) lattice planes. Since the cubic unit cell side length of Gd_2O_3 is 10.809 Å (PDF 43-1014), the corresponding interplanar distances for the reflections are calculated to be 3.12, 2.70, 1.91, and 1.63 Å. In agreement with the literature data, the (222) planes in cubic Gd_2O_3 correlate to the most intense signal in the FFT, and commonly these planes are clearly visible in the HR-TEM images. Crystalline particles could still be observed in samples stored in water at room temperature for several weeks. A representative TEM image of such a sample after storage in water for 2 months is shown to the right in Fig. 3. This TEM image shows separate nanoparticles with an estimated size of 4–5 nm indicating high stability in water solution. The corresponding FFT shows dots representing the (222), (400), (440), and (622) planes, respectively, in agreement with the FFT for freshly synthesized material. A reasonable stability in water was confirmed also by a ζ-Potential value of $+34.7 \pm 0.6$ mV. This positive charge indicates the presence of electrostatic repulsion between the particles which ensures colloidal stability. The size distribution of the nanoparticles presented in Fig. 4 was determined by studying approximately 100 nanoparticles on altogether 16 different images. For each nanoparticle, two orthogonal diameters were measured, and the mean value of the two was used as the size of the particle. Only nanoparticles with clearly apparent fringes were taken into account. The mean size of the nanoparticles in TEM was 4.7 ± 1.3 nm, a value that had not changed significantly 10 weeks after the synthesis (the right image in Fig. 3). What appeared to be "fragments" of nanoparticles could be seen on some images, especially in samples stored in water for longer time. Ostwald ripening, which causes large particles to grow by relocating material from smaller particles, is suggested to be a part of this fragmentation.

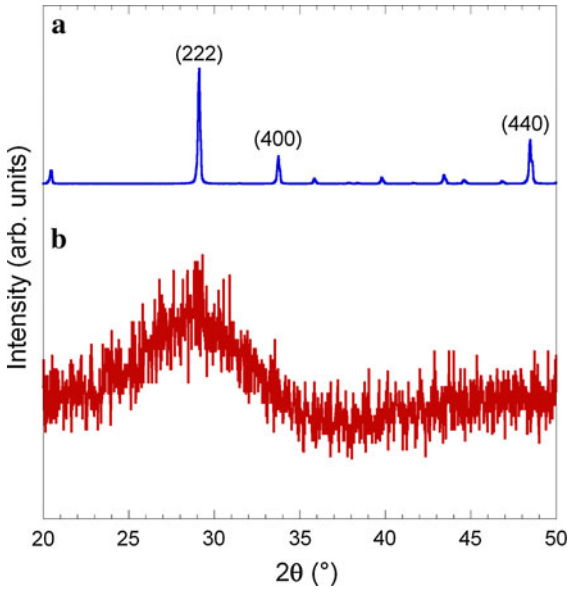

Fig. 2 Powder diffraction patterns of (*a*) a commercial Gd_2O_3 bulk powder and (*b*) Gd_2O_3

Dynamic light scattering (DLS) was used as a complementary technique to TEM to estimate the hydrodynamic radius of the Gd_2O_3 nanoparticles. Fifteen samples were analyzed using DLS. An important issue when analyzing the DLS results is the presence of large particles or loosely bound aggregates. Using unweighted DLS fits, the presence of larger aggregates was confirmed in all samples. Using number weighed fits, on the other hand, it was shown that clearly the majority of the particles have a hydrodynamic radius below 10 nm. From these number weighted fits, an indicative nanoparticle radius in single sampling correlation could be estimated to 6.9 ± 4.3 nm for newly synthesized nanoparticle suspensions; to 5.3 ± 2.9 nm 1 week after synthesis; and to 5.1 ± 3.4 nm 2 weeks after synthesis, as illustrated in Fig. 5. After 6 weeks, the mean radius had increased to 6.7 ± 4.7 nm.

Molecular composition

Infrared (IR) spectroscopy was used to study the vibrational modes of the precursor molecules and to identify molecular capping present at the surface of Gd_2O_3 nanoparticles. Theoretical IR spectroscopy calculations were based on three different gadolinium acetate complexes, as described in the "Computational details" section. Experimental IR spectra of the

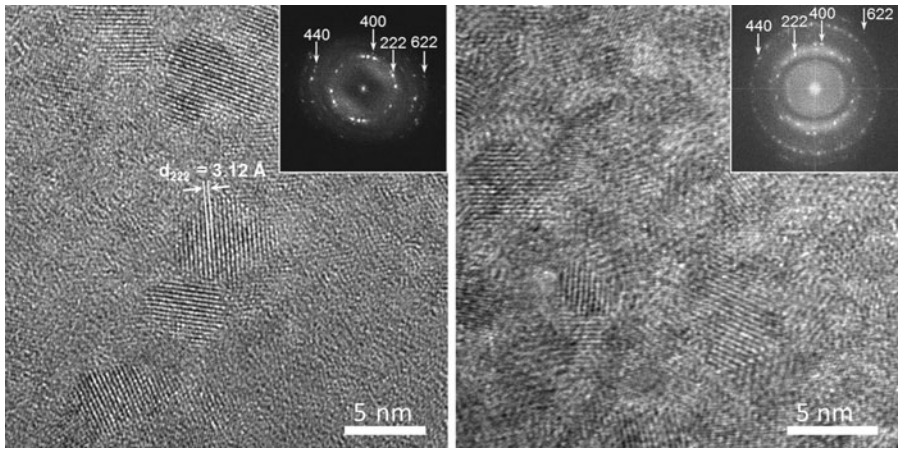

Fig. 3 Transmission electron microscope images of recently synthesized Gd_2O_3 nanoparticles (*left*) and a corresponding 2-month-old sample (*right*) together with their related fast fourier transforms (FFTs)

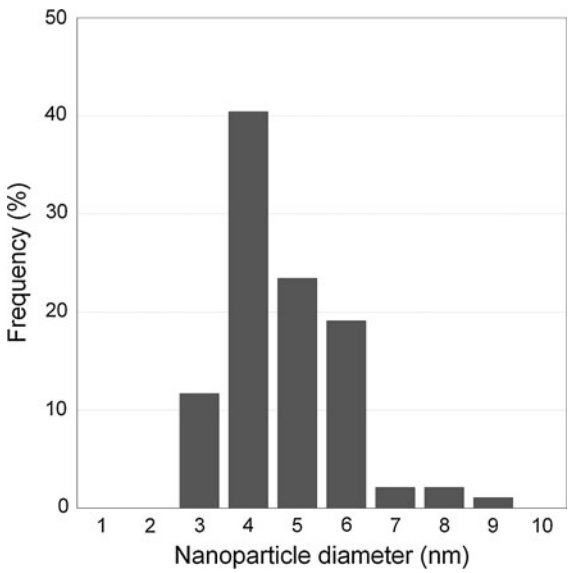

Fig. 4 Size distribution of Gd_2O_3 nanoparticles measured with TEM. The total column sum of all frequencies equals 100 %

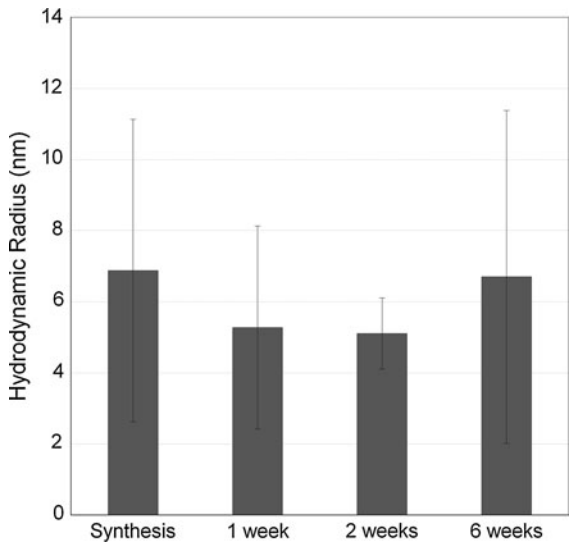

Fig. 5 Hydrodynamic radius of Gd_2O_3 nanoparticles studied with DLS. Measurements were performed directly after synthesis and 1, 2, and 6 weeks after synthesis

precursors TMAH and $Gd(OAc)_3$ and Gd_2O_3 nanoparticles are shown in Fig. 6a–c, respectively, and calculated spectra for the three different gadolinium acetate complexes are shown in Fig. 6d–f. Peak positions and assignments of the experimental and theoretical gadolinium acetate spectra in Fig. 6a and e are summarized in Table 1.

Our conclusion when comparing the experimental and calculated spectra of gadolinium acetate in Fig. 6a and d–f, respectively, is that the best overall agreement is found for $[Gd(OAc)_3(H_2O)_2]_2$ (Fig. 6e). The most prominent peaks in Fig. 6a and c–f are found in the range 1,400–1,600 cm^{-1} and are mainly assigned to originate from the antisymmetric, $\nu_{as}(COO^-)$, and symmetric, $\nu_s(COO^-)$, carboxylate stretching modes. It has been suggested by Nakamoto (1997), although contradicted by Edwards and Hayward (1968), that the separation (Δ) of these peaks can be used to interpret the mode of coordination of a carboxylate group to a metal cation. For $\Delta > 200$ cm^{-1} monodentate binding is expected, for $\Delta < 110$ cm^{-1} bidentate binding is expected, and for $140 < \Delta < 200$ bridging binding is expected. Furthermore, according to the literature concerning, the three gadolinium acetate complexes (Favas et al. 1980; Hatscher and Urland 2003; Smith and Ryan 1992), bidentate and bridging metal ion

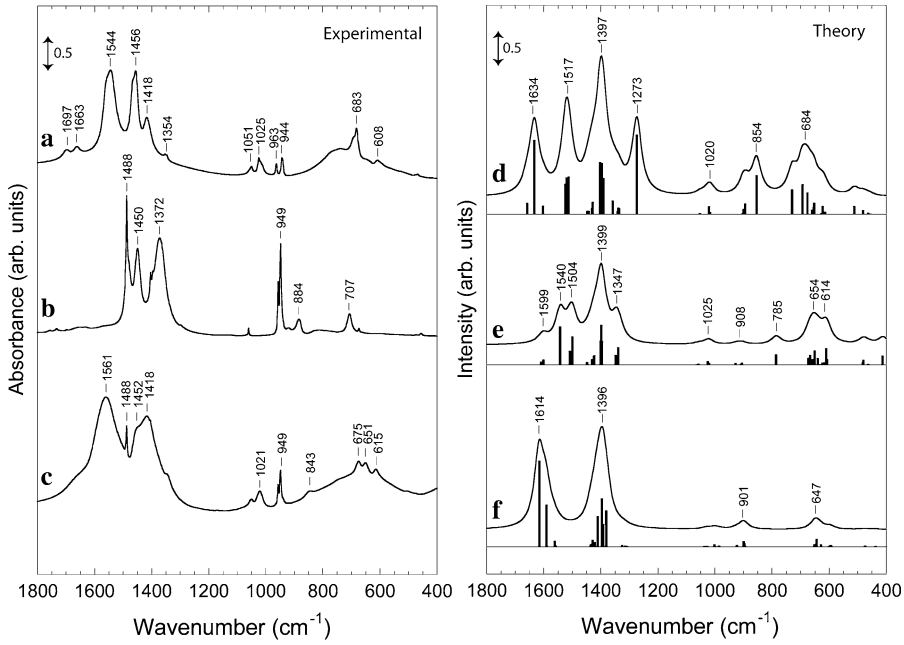

Fig. 6 Experimental transmission IR spectra of the precursors (*a*) $Gd(OAc)_3$, (*b*) tetramethyl ammonium hydroxide (TMAH), and (*c*) as-synthesized Gd_2O_3 nanoparticles and theoretically calculated spectra for (*d*) $[Gd(OAc)_4(H_2O)_2]^-$, (*e*) $[Gd(OAc)_3(H_2O)_2]_2$, and (*f*) $[Gd_2(OAc)_8]^{2-}$

Table 1 IR spectroscopy peak positions and assignments based upon the experimental measurement of gadolinium acetate and the calculated IR spectra of $[Gd(OAc)_3(H_2O)_2]_2$

Experimental ν (cm^{-1})	Theoretical ν (cm^{-1})	Assignment
1,697/1,663	1,599	$\delta_s(H_2O)$
1,544	1,540	$\nu_{as}(COO^-)$ bridge
	1,504	$\nu_{as}(COO^-)$ bidentate
1,456	1,399	$\nu_s(COO^-)$ bidentate, bridge, $\delta_{as}(CH_3)$
1,418		$\delta_{as}(CH_3)$
1,354	1,347	$\delta_s(CH_3)$
1,051; 1,025	1,025	$\rho(CH_3)$, δ(C sp_2, out of plane)
963; 944	908	ν(C–C)
	785	H_2O
683	654; 614	δ(O–C–O)

coordination are both present in gadolinium acetate and hence, carboxylate antisymmetric and symmetric stretch splits are expected in this study. The presence of two peaks originating form antisymmetric carboxylate stretching is observed in the theoretical spectra in Fig. 6e (1,540 and 1,504 cm^{-1}). The peaks originating from symmetric carboxylate stretching are overlapped generating one broad peak at 1,399 cm^{-1}.

The experimental spectrum for $Gd(OAc)_3$ in Fig. 6a presents three peaks in the wavenumber region of 1,400–1,600 cm^{-1}. The results from the theoretical calculations and the knowledge that two binding fashions are usually present in $Gd(OAc)_3$ make us interpret the broad peak at 1,544 cm^{-1} as to originate from two overlapping peaks both representing antisymmetric carboxylate stretching but from different coordination modes. The peak position of symmetric carboxylate stretching in gadolinium acetate is, according to the literature, somewhat contentious. Patil et al. (1968) have previously assigned a peak at about 1,420 cm^{-1} to symmetric carboxylate stretching and a peak at about 1,460 cm^{-1} to methyl deformation, whereas Karraker (1969) has done the opposite assignment attributing a peak at 1,450 cm^{-1} to symmetric carboxylate stretching and a peak at 1,412 cm^{-1} to asymmetric bending of CH_3. According to the results of the IR calculations and the observed peak intensities, the last mentioned assignment is to be preferred. In Fig. 6a, the peak intensity of the peak at 1,418 cm^{-1} is far too low to originate from carboxylate stretching and we thus assign the peak at 1,456 cm^{-1} to symmetric carboxylate stretching. A shoulder is present at a slightly higher wavenumber, again indicating the presence of two different binding modes and a small broadening of the peak, in agreement with the calculated spectra. Broadening is also a consequence of the presence of overlapping methyl bending peaks in the same wavenumber area and at 1,418 cm^{-1}. The wavenumber separation of

the antisymmetric and symmetric carboxylate stretching (Δ) in Fig. 6a is 88 cm^{-1} when using the maximum intensity of the unresolved peaks, primarily representing bidentate binding according to Nakamoto (1997). The corresponding approximate peak-to-peak separation in the calculated spectra is 123 cm^{-1}, a value positioned in the middle between the ranges for bridge and bidentate coordination. Significant peak broadening of the corresponding peaks is obvious also in the spectrum of Gd_2O_3 nanoparticles in Fig. 6c. Here, broadening occurs because of further overlap with C–H vibrations originating from TMAH as well as acetate methyl groups but probably also from gadolinium carbonates, which are formed on the nanoparticle surface. Carbonate presence is further validated by the existence of a weak carbonate bending structure at about 845 cm^{-1}. As observed in the theoretical and experimental analysis of gadolinium acetate spectra, splitting upon different binding character probably also appears inducing further broadening. The presence of acetate and carbonate species on the particle surface is likely to increase the nanoparticle stability. Uncapped Gd_2O_3 nanoparticles would not be stable enough to be treated in water. Compared to the spectrum in Fig. 6a, the peak intensity of the peak at 1,418 cm^{-1} in Fig. 6c has increased significantly. We therefore suggest this peak to originate from symmetric carboxylate stretching generating a wavenumber separation of 143 cm^{-1}, mainly corresponding to a bridging coordination in agreement with our earlier studies of Gd_2O_3 functionalized with citric acid (Söderlind et al. 2005).

It is evident, by comparing the spectra in Fig. 6b and c, that TMAH precursors are still present in newly synthesized and centrifuge washed Gd_2O_3. This is observed as two very distinctive TMAH peaks at about 1,488 and 949 cm^{-1}. When changing ethyl acetate to ethanol in the last wash step, TMAH is removed from the Gd_2O_3 sample which is clearly shown by elimination of the TMAH peaks in the IR spectrum (Supplementary information). Bands corresponding to the cubic phase Gd–O vibration have earlier been identified at about 550 and 440 cm^{-1}, when studying Gd_2O_3 waveguiding thin films (Guo et al. 2004b; García-Murillo et al. 2001), sol–gel synthesized Gd_2O_3 nanocrystals (Guo et al. 2004a), and Eu-doped Gd_2O_3 nanocrystals synthesized by a sol-lyophilization process (Louis et al. 2003). In the present case, though, the Gd–O vibration is absent, most likely as a consequence of the small size of the nanoparticles. We have scanned the literature to find these vibrations in other cases when studying Gd_2O_3 nanoparticles, but to our knowledge the particular Gd–O vibrations have not been observed for Gd_2O_3 nanoparticles of this small size below 10 nm in diameter. Furthermore, IR spectra have previously shown to be crystallite size dependent. Bednarkiewicz et al. (2006) concluded that the intensity of vibrational bands decreases with decreasing particle size when studying $NaGdF_4$ nanocrystals. Peak intensity decrease was followed also by bandwidth broadening, and the size effect was most pronounced for low-energy frequencies. Peak intensity decrease and broadening upon reduced particle size were noticed also by Zhang et al. (2004). Heating Gd_2O_3 nanoparticle samples is tightly coupled to crystal growth (Louis et al. 2003). When samples heated to 1,100 °C in the TG study were examined with IR spectroscopy, clear peaks at about 436 and 542 cm^{-1} appeared as a consequence of increased nanoparticle size (Supplementary information). The observed IR spectrum showed that the sample was free from carbonates/acetates, and the Gd–O peak positions were consistent with the corresponding peak positions earlier found when investigating commercial Gd_2O_3 nanopowder (diam $<$ 100 nm).

Near-edge X-ray absorption fine structure (NEXAFS) spectroscopy was used in combination with XPS to study the molecular composition of the Gd_2O_3 nanoparticles. The experimental C K-edge spectra of Gd_2O_3 and Gd acetate are shown in Fig. 7 together with the C K-edge spectra of $[Gd(OAc)_3(H_2O)_2]_2$ and the isolated acetate group obtained from the theoretical calculations. A summary of the assignments of the peaks is shown in Table 2.

The Gd_2O_3 spectrum (Fig. 7a) shows two major peaks originating from acetate and carbonate groups, and several minor features. The very sharp peak at 288.3 eV is assigned to C1s $\rightarrow \pi^*_{C=O}$ transitions in the acetate unit in agreement with the Gd acetate spectrum (Fig. 7b).

Complex binding of the acetate unit to metal ions have earlier shown to alter the NEXAFS spectra of the acetate group (Armbruster et al. 2009; Plaschke et al. 2004). Complexation is thought to induce an intensity decrease in the main acetate peak and at the same time a shoulder appears at slighter lower energy. Theoretical spectra of isolated acetate and complex bound acetate were studied to investigate the effect of complexation (Fig. 7c, d). The intensity of the free

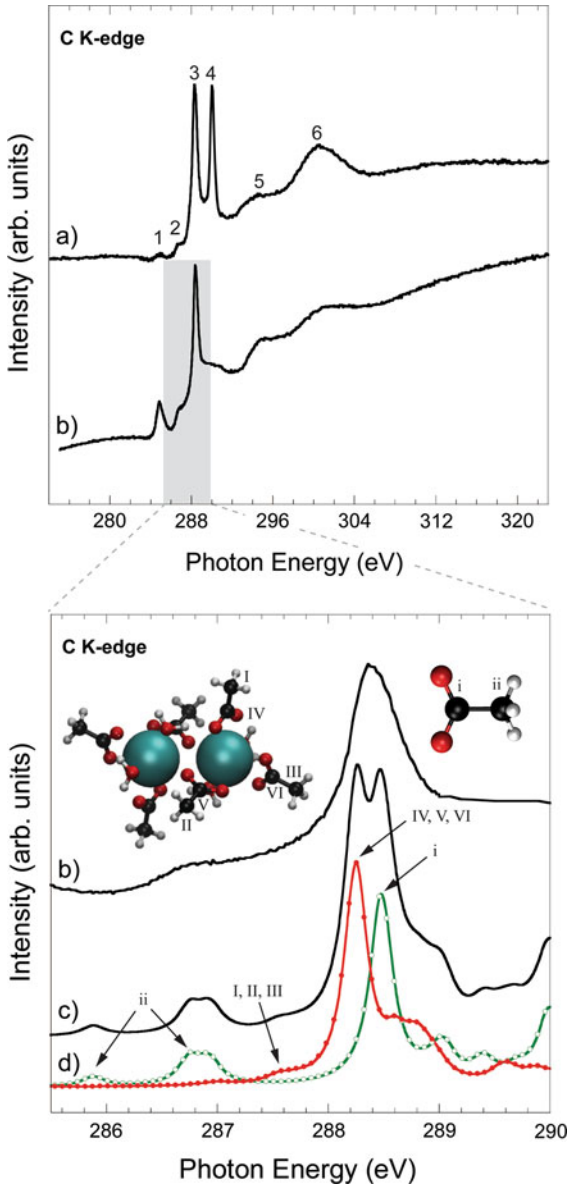

Fig. 7 Experimental C K-edge NEXAFS spectra of (*a*) Gd_2O_3 nanoparticles and (*b*) the precursor Gd acetate with peak numbers referring to assignments made in Table 2. Theoretically calculated spectra of isolated acetate (*green line*, hollow markers) and the coordination complex $[Gd(OAc)_3(H_2O)_2]_2$ (*red line*, filled markers) are shown in (*d*) together with the sum of these two spectra in (*c*)

acetate spectrum has been multiplied by 6 in order to match the stoichiometric ratio of the gadolinium complex. From the elements in the imaginary part of the response vectors, absorption peaks could be attributed to specific atoms in the molecule. The results obtained from these theoretical calculations in

Table 2 Assignment in the C K-edge spectra of Gd_2O_3 nanoparticles and gadolinium acetate

Peak number	Excitation energy (eV)	Assignment
1	284.9	C1s $\rightarrow$ $\pi^*_{C=C}$
2	286.8	C1s $\rightarrow$ $\pi^*_{C=O}$ acetate
3	288.3	C1s $\rightarrow$ $\pi^*_{C=O}$ acetate
4	290	C1s $\rightarrow$ $\pi^*_{C=O}$ carbonate
5	294.3	C1s $\rightarrow$ σ^*_{C-C} acetate
6	300.4	C1s $\rightarrow$ σ^*_{C-O} acetate/carbonate

Fig. 7d show that there are major differences between the spectra of complex bound (red curve, filled markers) and isolated acetate (green curve, hollow markers). The main peak for isolated acetate is positioned at slightly higher photon energy, as compared to the same peak for the metal bound acetate. Furthermore, two broad structures clearly appear at the low-energy side of the main peak in the spectra of the free acetate. These two structures, marked with ii in Fig. 7d, are attributed to the methyl carbon of the acetate, which is also the case for the lower intensity feature marked with roman numerals (I, II, III) in the spectra of the metal coordinated acetate in the same figure.

The experimental spectrum of Gd acetate in Fig. 7b agrees with the combined spectra of isolated and complex bound acetate in Fig. 7c. The broad $\pi^*_{C=O}$ peak in the C K-edge Gd acetate peak in the experimental spectrum is thus suggested to be composed of two overlapping peaks corresponding to this transition of the free and complex bound acetate, respectively, as based on the theoretical spectra in Fig. 7d. This interpretation is furthermore supported by the presence of a broad feature at around 286.8 eV in Fig. 7b. As based upon these results, it is likely that the condition in solution is dynamic, with several different acetate complexes coexisting with free acetate groups.

It is well known that a Gd_2O_3 nanoparticle readily reacts with atmospheric CO_2 to form carbonates on the surface (Kaltsoyannis and Scott 1999; Baltrusaitis et al. 2011), and the sharp peak at about 290 eV is assigned to C1s $\rightarrow$ $\pi^*_{C=O}$ originating from carbonate species (Koprinarov et al. 1998; Urquhart and Ade 2002; Lippitz et al. 1996). The minor peak at photon energy at 285 eV usually is attributed to C1s $\rightarrow$ $\pi^*_{C=C}$ transitions. However, no C=C bonds are expected in Gd acetate, and the peak most likely

originates from chemical impurities in the precursor compound. The two broad peaks at higher energies in the spectrum of Gd acetate in Fig. 7 both originate from σ^* resonances. Peak number 5 (294 eV) can be assigned to C–C bonds (σ^*_{C-C}) and possibly also to C–N (σ^*_{C-N}) bonds, whereas peak number 6 (300 eV) is assigned to σ^*_{C-O} in acetate (Graf et al. 2009; Hasselström et al. 1998). In the nanoparticle spectrum, the presence of carbonates on the nanoparticle surface partly alters the line shape and increases the intensity of the last mentioned σ^* resonance, since carbonate σ^*_{C-O} transitions overlap with the corresponding transition in acetate (Stöhr 1992). Carbonate formation is further evidenced by the O K-edge spectrum in Fig. 8 with the corresponding peak assignments given in Table 3. In the Gd_2O_3 nanoparticle O K-edge spectrum in Fig. 8a, five peaks are observed. The first two peaks (1 and 2) overlap. The O K-edge NEXAFS spectrum of Gd acetate in Fig. 8b show one sharp peak at 531.9 eV which, together with Peak 1 in Fig. 8a, is assigned to the O1s $\rightarrow$ $\pi^*_{C=O}$ transition in the acetate unit. Peak broadening in this region has earlier been observed by Koprinarov et al. (1998) when studying the stepwise degradation of carbonates to carbonyls. The carbonate $\pi^*_{C=O}$ transition partly coincides with the acetate $\pi^*_{C=O}$ as shown in the magnified inset in Fig. 8 (Lippitz et al. 1996; Hasselström et al. 1998). Broad σ^* resonances are observed at higher energies (Peaks 3–5). Peak 3 at 536 eV is assigned to the O1s $\rightarrow$ σ^*_{Gd-O} transition in Gd_2O_3. According to Lee et al. (2010) and Nachimuthu et al. (2004), the O K-edge NEXAFS spectrum of Gd_2O_3 shows two broad peaks centered at 532 and 537 eV. In our case, the lower photon energy feature is presumably concealed as a consequence of the carbonate and acetate overlaps. Peak numbers 4 and 5 are both assigned to O1s $\rightarrow$ σ^*_{C-O} transition. These transitions originate from acetate as well as carbonate groups, and, moreover, splitting of the σ^* system caused by interaction of two adjacent C=O bonds (Stöhr 1992) is likely to occur. The NEXAFS Gd M-edge spectrum in Fig. 9 shows two peaks positioned at 1,180 and 1,212 eV, respectively. These peaks are assigned to the 3*d*–4*f* transition, and the separation between the peaks is due to the spin–orbit splitting of the $3d_{5/2}$ and $3d_{3/2}$ level. The reason to the multiplet feature in each of the peaks is the spin–orbit moment coupling of 3*d* and 4*f* states (Thole et al. 1985). The Gd N-edge

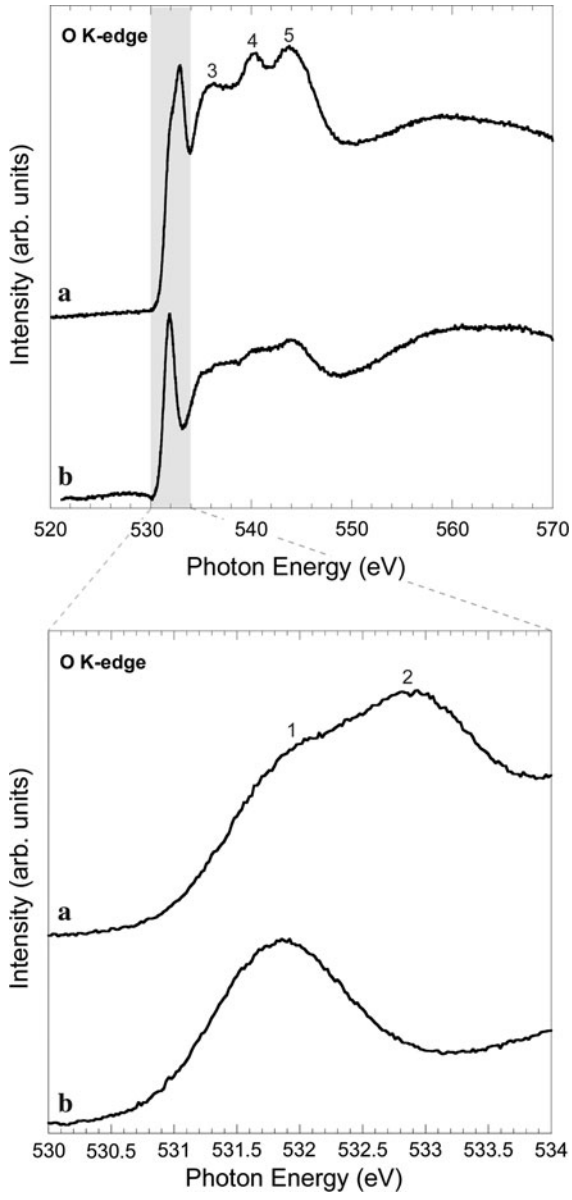

Fig. 8 O K-edge NEXAFS spectra of (*a*) Gd_2O_3 nanoparticles and (*b*) the precursor Gd acetate with peak numbers referring to assignments made in Table 3

spectrum in Fig. 9 involves pre-threshold peaks and a giant peak, in good agreement with the *4d–4f* transition of gadolinium (Ogasawara and Kotani 1995; Takayama et al. 2002).

The chemical composition of Gd_2O_3 nanoparticles was studied with X-ray photoelectron spectroscopy (XPS), and the experimental data were analyzed using curve fitting. The spectra of O (1s), Gd (3d), and C (1s)

Table 3 Assignments in the O K-edge spectra of Gd_2O_3 nanoparticles and gadolinium acetate

Peak number	Excitation energy (eV)	Assignment
1	531.9	O1s $\rightarrow \pi^*_{C=O}$ acetate
2	532.9	O1s $\rightarrow \pi^*_{C=O}$ carbonate
3	536.3	O1s $\rightarrow \sigma^*_{Gd-O}$ in Gd_2O_3
4	540.5	O1s $\rightarrow \sigma^*_{C-O}$ acetate/carbonate
5	543.6	O1s $\rightarrow \sigma^*_{C-O}$ acetate/carbonate

of Gd_2O_3 nanoparticles are presented in Figs. 10, 11, and 12, respectively. The O (1s) spectrum in Fig. 10 is dominated by one major peak positioned at 531.9 eV. Two small peak features are also observed at 529.5 and 533.6 eV, respectively. The experimental Gd/O ratio, as calculated from the total areas of Gd 3d and O 1s peaks in the wide scan XPS spectrum, was estimated to be 0.08 while the stoichiometric ratio of pure Gd_2O_3 is 0.67. In nanoparticles capped with organic material, the signal from the core will be suppressed, however, to an extent that depends on both the thickness of the capping layer as well as on the kinetic energy of the electrons, i.e., the X-ray photon energy. In other words, the inelastic mean free path (IMFP) of an electron is dependent on its kinetic energy according to the *Universal curve* (Attard and Colin 1998), and the distance that the electron has to travel inside the material to reach the detector is among other things dependent on the capping layer thickness. Gd electrons emitted in the photoelectron process using 1,300 eV in photon energy have a kinetic energy lower than 100 eV. Emitted O electrons originating from the Gd_2O_3 core oxygen also have a kinetic energy close to 100 eV, when using a photon energy of 650 eV. Cumpson (2001) has suggested a way to estimate IMFPs of electrons in polymers and other organic materials at different kinetic energies. Using his method and the given kinetic energies, the IMFPs of both O and Gd electrons are estimated to about 5 Å. Still, a small amount of oxygen originating from the nanoparticle core is observed at 529.5 eV (Raiser and Deville 1991; Frohlich et al. 2006). The main peak at 531.9 eV in the O 1s spectra is mainly attributed to oxygens in acetate and carbonate groups which have similar binding energies (Mercier et al. 2006; Gonzalez-Elipe et al. 1990). Moreover, the small peak above 536 eV is most likely related to hydroxide groups and/or water adsorbed to the nanoparticle surface (Jeon and Hwang 2003; Hugenschmidt et al. 1994; Chiba et al. 2000).

With the relatively high-sensitivity factor of Gd 3d taken into account, the low intensity of the Gd 3d peaks in Fig. 11 further verifies a suppressed Gd signal from the core of nanoparticle. The peak positions of

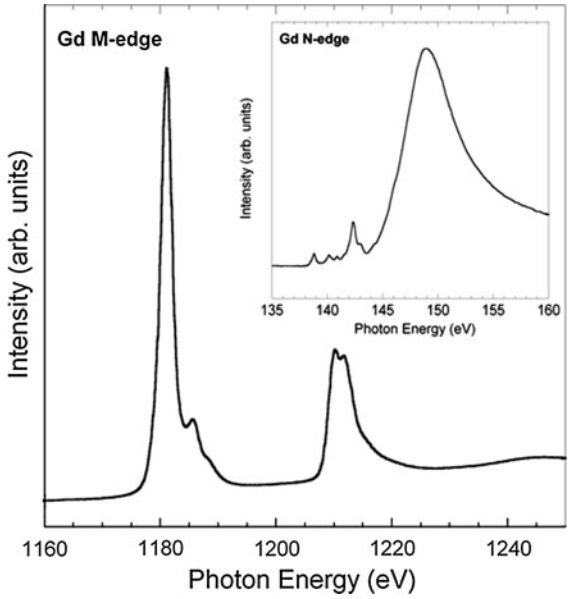

Fig. 9 Gd M-edge and Gd N-edge (*inset*) NEXAFS spectra of Gd_2O_3 nanoparticles

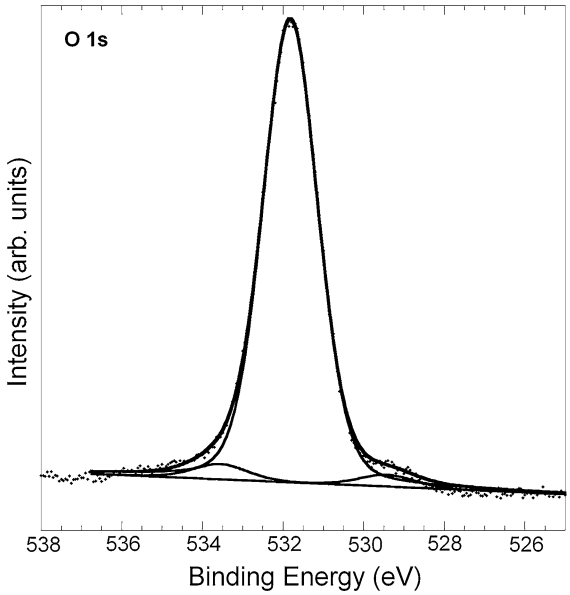

Fig. 10 O1s XPS spectrum of Gd_2O_3 nanoparticles

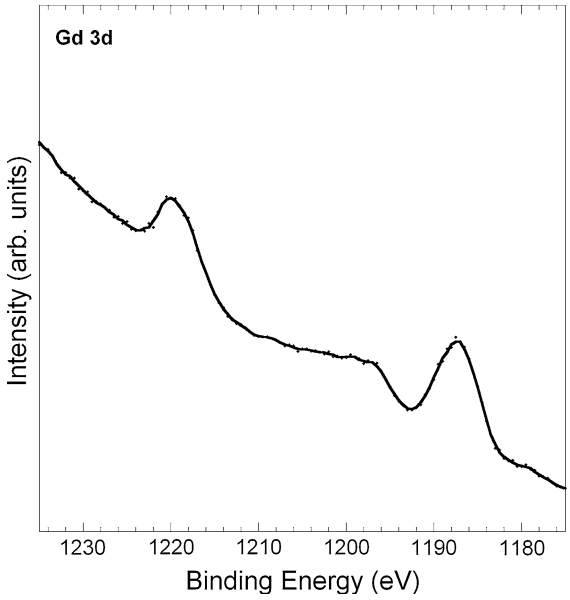

Fig. 11 Smooth curve fitted Gd 3d XPS spectrum of Gd_2O_3 nanoparticles

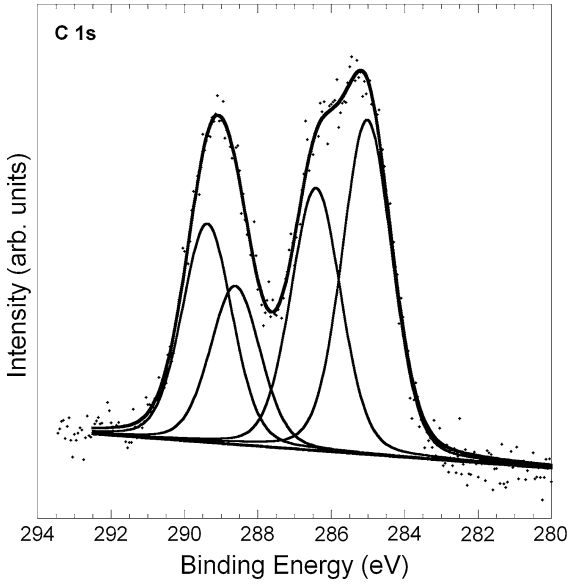

Fig. 12 C 1s XPS spectrum of Gd_2O_3 nanoparticles

the 3d lines in Gd_2O_3 are shifted to higher binding values (1,188 and 1,220 eV) compared to the corresponding elemental Gd $3d_{5/2}$ and Gd $3d_{3/2}$ at 1,186 and 1,218 eV, respectively, as expected. The spin orbit splitting is 32 eV in agreement with previously reported data for Gd_2O_3 (Raiser and Deville 1991). The C (1s) XPS spectrum of Gd_2O_3 nanoparticles is shown in Fig. 12 with four peaks fitted to the experimental data. Chemical shifts of the carbon peaks are known to probe the chemical environment by means of nearest and next nearest neighbors (Watts and Wolstenholme 2003). The commonly observed chemical shifts in C (1s) spectra are dominated by the very nearest neighbor atoms. According to Gelius et al. (1970), a shift of 0.3 eV to higher binding energies is expected for methyl carbon in an acetate group compared to a reference hydrocarbon value of 285 eV. This fairly small shift is not obvious in our spectra, and the peak at 285 eV is attributed mainly to methyl carbon present in Gd acetate but also to an additional contribution of adventitious aliphatic carbon present as contamination. The peak at 286.4 is primarily attributed to nitrogen bound carbon present in TMAH. The presence of TMAH was also confirmed with IR spectroscopy. Hydroxyl bound carbons have similar binding energies and may also be part of the same peak at 286.4 eV. Peaks associated with acetate carbonyl carbon (288.6 eV) and carbonate carbon (289.2 eV) are both observed at higher binding energies. The peak-to-peak separation of the two carbons in acetate (285 and 288.6 eV) equals 3.6 eV, which is a value in agreement with previous reported data concerning acetate binding energies on metal oxides (Vohs and Barteau 1988).

In conclusion, the results from NEXAFS, XPS, and IR spectroscopy validate that the nanoparticle surface is covered with acetate and carbonate groups which are expected to stabilize the Gd_2O_3 core in water.

The thermogravimetric (TG) curve in Fig. 13 shows about 40 % mass loss of an as-synthesized and air-dried Gd_2O_3 nanoparticle sample upon heating

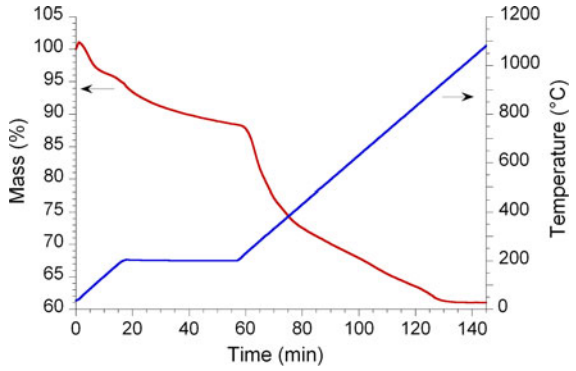

Fig. 13 Mass change upon heating of Gd_2O_3 nanoparticles in the TG measurement

to 1,100 °C from room temperature in He. Qualitative data obtained by mass spectrometry showed that already at low temperatures (~75 °C) H_2O is emitted, which is attributed to adsorbed water. At ~260 °C, decomposition of organic species starts giving emission of mainly H_2O, CO_2, and CO/N_2. The emission of CO_2 continues up to about 900 °C indicating decomposition of carbonates. The TG-MS data support the general picture of the chemical composition of the nanoparticles as presented above.

Relaxation studies

Relaxation measurements were performed on Gd_2O_3 nanoparticles in MilliQ, and the relaxivity results were compared with data obtained for an aqueous solution of $GdCl_3$ and a common commercial contrast agent (Gd-DTPA, Magnevist). Plots of the inverted relaxation times T1 and T2 vs. the Gd concentrations are shown in Figs. 14 and 15, respectively. The absolute r_1 and r_2 values, and the relative r_2/r_1 ratios, for the studied samples are listed in Table 4. As one would expect, the r_1 and r_2 relaxivities of Gd-DTPA (3.5 and 4.1 mM^{-1} s^{-1}, respectively) are low compared to those for free Gd^{3+} ions in water (7.9 and 9.0 mM^{-1} s^{-1}, respectively). This observation is true for all chelate type contrast agent and is a consequence of the increased activation barrier and thereby the slower water exchange rates for complexes (Helm and Merbach 2005). The relaxivity values for the Gd_2O_3 nanoparticles (6.9 and 7.9 mM^{-1} s^{-1}) are remarkably close to those for free Gd^{3+} ions, and about twice as high as those for Gd-DTPA. It is clear that compared to earlier studied dialyzed polyol synthesized Gd_2O_3 nanoparticles in MilliQ, which have shown a smaller difference in relaxivity compared to Gd-DTPA (Engström et al. 2006; Ahrén et al. 2010), the present nanoparticles appear to have considerably more efficient MR contrast enhancement properties. The relative r_2/r_1 ratio for Gd_2O_3 is close to one (Table 4), which is preferable for a positive contrast agent.

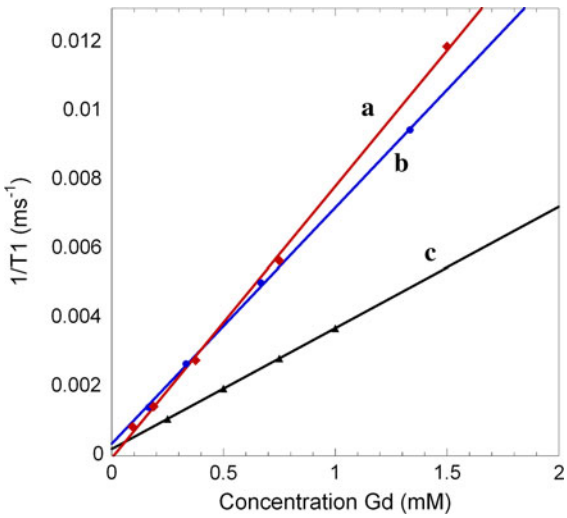

Fig. 14 Experimentally measured longitudinal relaxation of (*a*) $GdCl_3$ in MilliQ water, (*b*) Gd_2O_3 nanoparticles in MilliQ water, and (*c*) Magnevist

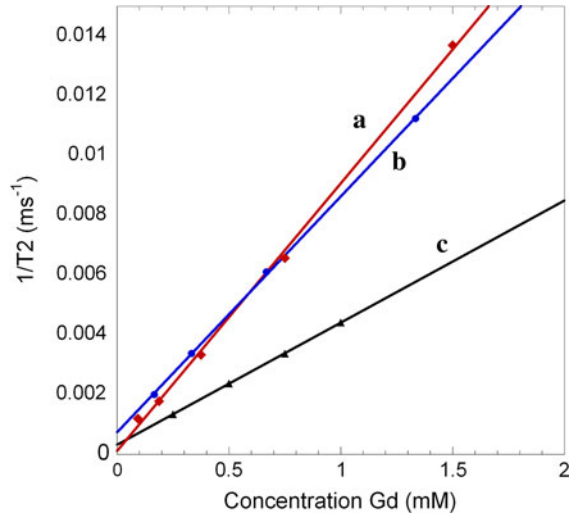

Fig. 15 Experimentally measured transverse relaxation of (*a*) $GdCl_3$ in MilliQ water, (*b*) Gd_2O_3 nanoparticles in MilliQ water, and (*c*) Magnevist

Table 4 r_1 and r_2 relaxivities together with the r_2/r_1 ratio for $GdCl_3$, Gd_2O_3, and Magnevist

Agent	r_1 (mM^{-1} s^{-1})	r_2 (mM^{-1} s^{-1})	r_2/r_1
$GdCl_3$	7.9	9	1.14
Gd_2O_3	6.9	7.9	1.14
Magnevist	3.5	4.1	1.17

Conclusion

It has been demonstrated that small Gd_2O_3 nanocrystals can be synthesized via a simple and fast polyol-free route at room temperature using a method previously developed for the synthesis of ZnO. The nanoparticle core size, as determined by TEM, was

approximately 4–5 nm, and the hydrodynamic radius of the particles dispersed in water, as measured by DLS, was of the order 5–10 nm. The chemical composition of the Gd_2O_3 nanoparticles was studied with several spectroscopic techniques (IR, NEXAFS, and XPS) and with TG-MS. On the basis of IR, NEXAFS, and XPS, carbonate formation on the nanoparticle surface was verified inducing a suppressed nanoparticle Gd signal in XPS. The nanoparticle surface was also shown to contain acetate molecules stabilizing the particles in water solution, as well as adsorbed water. The interpretation of the experimental IR data was corroborated by theoretical calculations on three different gadolinium acetate structures, of which the dimer complex ($[Gd(OAc)_3(H_2O)_2]_2$ was found to be the most relevant one for the studied systems. The MR properties, as measured with a benchtop TD-NMR analyzer, yielded the values 6.9 and 7.9 $mM^{-1}\ s^{-1}$ for r_1 and r_2, respectively. These values are considerably higher than those found for the Gd-DTPA chelate and in the same range as those for free Gd^{3+} in water.

Acknowledgments The present work is financed by grants from VINNOVA within the program Innovations for future health, Multifunctional Nanoprobes for Biomedical Visualization Dnr: 2008-03011, the Centre in Nanoscience and Technology at LiTH (CeNano) and Swedish research council (Grant No. 621-2010-5014). M.L. thanks SERC (Swedish e–Science Research Center) for funding and SNIC for providing computer resources. We also thank A. Preobrajenski, manager for Beamline D1011 at MaxLab in Lund, for the assistance during our NEXAFS measurements.

References

Aagaard Jensen HJ, Ågren H, Helgaker T, Jørgensen P et al (2005) DALTON, a molecular electronic structure program, Release Dalton (2011), see http://daltonprogram.org/

Ahrén M, Selegård L, Klasson A, Söderlind F, Abrikossova N, Skoglund C, Bengtsson T, Engström M, Käll P-O, Uvdal K (2010) Synthesis and characterization of PEGylated Gd_2O_3 nanoparticles for MRI contrast enhancement. Langmuir 26(8):5753–5762

Alexis F, Pridgen E, Molnar LK, Farokhzad OC (2008) Factors affecting the clearance and biodistribution of polymeric nanoparticles. Mol Pharm 5(4):505–515

Armbruster MK, Schimmelpfennig B, Plaschke M, Rothe J, Denecke MA, Klenze R (2009) Metal-ion complexation effects in C 1s-NEXAFS spectra of carboxylic acids—evidence by quantum chemical calculations. J Electron Spectrosc Relat Phenom 169(1):51–56

Attard G, Colin B (1998) Surfaces. Oxford chemistry primers. Oxford University Press, New York

Baltrusaitis J, Schuttlefield J, Zeitler E, Grassian VH (2011) Carbon dioxide adsorption on oxide nanoparticle surfaces. Chem Eng J 170(2–3):471–481

Becke AD (1993) Density-functional thermochemistry. III. The role of exact exchange. J Chem Phys 98(7):5648–5652

Bednarkiewicz A, Maczka M, Strek W, Hanuza J, Karbowiak M (2006) Size dependence on infrared spectra of NaGdF4 nanocrystals. Chem Phys Lett 418(1–3):75–78

Bolskar RD, Benedetto AF, Husebo LO, Price RE, Jackson EF, Wallace S, Wilson LJ, Alford JM (2003) First soluble M@C60 derivatives provide enhanced access to metallofullerenes and permit in vivo evaluation of Gd@C60 [C(COOH)2]10 as a MRI contrast agent. J Am Chem Soc 125(18):5471–5478

Boyd RW (2003) Nonlinear optics, 2nd edn. Academic Press, New York

Bridot JL, Faure AC, Laurent S, Riviere C, Billotey C, Hiba B, Janier M, Josserand V, Coll JL, Vander Elst L, Muller R, Roux S, Perriat P, Tillement O (2007) Hybrid gadolinium oxide nanoparticles: multimodal contrast agents for in vivo imaging. J Am Chem Soc 129(16):5076–5084

Caravan P, Ellison JJ, McMurry TJ, Lauffer RB (1999) Gadolinium(III) chelates as MRI contrast agents: structure, dynamics, and applications. Chem Rev 99(9):2293–2352

Chaput F, Lerouge F, Tusseau-Nenez S, Coulon P-E, Dujardin C, Denis-Quanquin S, Mpambani F, Parola S (2011) Rare earth fluoride nanoparticles obtained using charge transfer complexes: a versatile and efficient route toward colloidal suspensions and monolithic transparent xerogels. Langmuir 27(9):5555–5561

Chiba K, Ohmori R, Tanigawa H, Yoneoka T, Tanaka S (2000) H_2O trapping on various materials studied by AFM and XPS. Fusion Eng Des 49–50:791–797

Cumpson PJ (2001) Estimation of inelastic mean free paths for polymers and other organic materials: use of quantitative structure–property relationships. Surf Interface Anal 31(1):23–34

Dolg M, Stoll H, Savin A, Preuss H (1989) Energy-adjusted pseudopotentials for the rare earth elements. Theor Chim Acta 75(3):173–194

Dunning TH (1989) Gaussian basis sets for use in correlated molecular calculations. I. The atoms boron through neon and hydrogen. J Chem Phys 90(2):1007–1023

Edwards DA, Hayward RN (1968) Transition metal acetates. Can J Chem 46(22):3443–3446

Ekström U, Norman P (2006) X-ray absorption spectra from the resonant-convergent first-order polarization propagator approach. Phys Rev A 74(4):042722

Engström M, Klasson A, Pedersen H, Vahlberg C, Käll P-O, Uvdal K (2006) High proton relaxivity for gadolinium oxide nanoparticles. Magn Reson Mater Phys Biol Med 19(4):180–186

Evanics F, Diamente PR, van Veggel FCJM, Stanisz GJ, Prosser RS (2006) Water-soluble GdF_3 and GdF_3/LaF_3 nanoparticles—physical characterization and NMR relaxation properties. Chem Mater 18(10):2499–2505

Favas MC, Kepert DL, Skelton BW, White AH (1980) Crystal structure of gadolinium(III) acetate tetrahydrate. Stereo-chemistry of the nine-co-ordinate [M(bidentate

ligand)$_3$(unidentate ligand)$_3$]$^{+/-}$ system. J Chem Soc Dalton Trans 3:454–458

Fortin M-A, Petoral RM Jr, Söderlind F, Klasson A, Engström M, Veres T, Käll P-O, Uvdal K (2007) Polyethylene glycol-covered ultra-small Gd_2O_3 nanoparticles for positive contrast at 1.5 T magnetic resonance clinical scanning. Nanotechnology 18(39):395501

Frisch MJ (2003) Gaussian 03. Revision B05. Gaussian, Pittsburgh

Frohlich K, Luptak R, Dobrocka E, Husekova K, Cico K, Rosova A, Lukosius M, Abrutis A, Pisecny P, Espinos JP (2006) Characterization of rare earth oxides based MOSFET gate stacks prepared by metal-organic chemical vapour deposition. Mater Sci Semicond Process 9(6): 1065–1072

García-Murillo A, Le Luyer C, Dujardin C, Pedrini C, Mugnier J (2001) Elaboration and characterization of Gd_2O_3 waveguiding thin films prepared by the sol-gel process. Opt Mater 16(1–2):39–46

Gelius U, Hedén PF, Hedman J, Lindberg BJ, Manne R, Nordberg R, Nordling C, Siegbahn K (1970) Molecular spectroscopy by means of ESCA III. Carbon compounds. Phys Scr 2(1–2):70–80

Geraldes CF, Laurent S (2009) Classification and basic properties of contrast agents for magnetic resonance imaging. Contrast Media Mol Imaging 4(1):1–23

Gonzalez-Elipe AR, Espinos JP, Fernandez A, Munuera G (1990) XPS study of the surface carbonation/hydroxylation state of metal oxides. Appl Surf Sci 45(2):103–108

Graf N, Yegen E, Gross T, Lippitz A, Weigel W, Krakert S, Terfort A, Unger WES (2009) XPS and NEXAFS studies of aliphatic and aromatic amine species on functionalized surfaces. Surf Sci 603(18):2849–2860

Guo H, Dong N, Yin M, Zhang W, Lou L, Xia S (2004a) Visible upconversion in rare earth ion-doped Gd_2O_3 nanocrystals. J Phys Chem B 108(50):19205–19209

Guo H, Yang X, Xiao T, Zhang W, Lou L, Mugnier J (2004b) Structure and optical properties of sol-gel derived Gd_2O_3 waveguide films. Appl Surf Sci 230(1–4):215–221

Gustafsson H, Ahrén M, Söderlind F, Córdoba Gallego JM, Käll P-O, Nordblad P, Westlund P-O, Uvdal K, Engström M (2011) Magnetic and electron spin relaxation properties of $(Gd_xY_{1-x})_2O_3$ $(0 \leq x \leq 1)$ nanoparticles synthesized by the combustion method. Increased electron spin relaxation times with increasing yttrium content. J Phys Chem C 115(13):5469–5477

Hasselström J, Karis O, Weinelt M, Wassdahl N, Nilsson A, Nyberg M, Pettersson LGM, Samant MG, Stöhr J (1998) The adsorption structure of glycine adsorbed on Cu(110); comparison with formate and acetate/Cu(110). Surf Sci 407(1–3):221–236

Hatscher ST, Urland W (2003) Unexpected appearance of molecular ferromagnetism in the ordinary acetate [{Gd(OAc)$_3$(H$_2$O)$_2$–2]·4H$_2$O. Angew Chem Int Ed 42(25): 2862–2864

Helm L, Merbach AE (2005) Inorganic and bioinorganic solvent exchange mechanisms. Chem Rev 105(6):1923–1960

Hifumi H, Yamaoka S, Tanimoto A, Citterio D, Suzuki K (2006) Gadolinium-based hybrid nanoparticles as a positive MR contrast agent. J Am Chem Soc 128(47):15090–15091

Hugenschmidt MB, Gamble L, Campbell CT (1994) The interaction of H_2O with a TiO_2(110) surface. Surf Sci 302(3):329–340

Jeon S, Hwang H (2003) Effect of hygroscopic nature on the electrical characteristics of lanthanide oxides (Pr_2O_3, Sm_2O_3, Gd_2O_3, and Dy_2O_3). J Appl Phys 93(10):6393–6395

Kaltsoyannis K, Scott P (1999) The f elements. Oxford chemistry primers. Oxford University Press, Oxford

Karraker DG (1969) Thiourea-lanthanide acetate complexes. J Inorg Nucl Chem 31(9):2833–2839

Kauczor J, Jørgensen P, Norman P (2011) On the efficiency of algorithms for solving Hartree–Fock and Kohn–Sham response equations. J Chem Theory Comput 7(6):1610–1630

Kim J, Jung Y, Lee J-K (2010) Synthesis and characterization of hollow nanoparticles of crystalline Gd_2O_3. J Nanopart Res 13(6):2311–2318

Koprinarov I, Lippitz A, Friedrich JF, Unger WES, Wöll C (1998) Oxygen plasma induced degradation of the surface of poly(styrene), poly(bisphenol-A-carbonate) and poly(ethylene terephthalate) as observed by soft X-ray absorption spectroscopy (NEXAFS). Polymer 39(14):3001–3009

Lai H, Bao A, Yang Y, Tao Y, Yang H (2008) Correlation of photoluminescence of (La, Ln) PO_4:Eu^{3+} (Ln = Gd and Y) phosphors with their crystal structures. J Nanopart Res 10(8):1355–1360

Lauffer RB (1987) Paramagnetic metal complexes as water proton relaxation agents for NMR imaging: theory and design. Chem Rev 87(5):901–927

Lee WJ, Cho MH, Kim YK, Baeck JH, Jeong IS, Jeong K, Chung KB, Kim SY, Ko DH (2010) Changes in Gd_2O_3 films grown on Si(100) as a function of nitridation temperature and Zr incorporation. Thin Solid Films 518(6): 1682–1688

Lippitz A, Koprinarov I, Friedrich JF, Unger WES, Weiss K, Wöll C (1996) Surface analysis of metallized poly(bisphenol A carbonate) films by X-ray absorption spectroscopy (NEXAFS). Polymer 37(14):3157–3160

Louis C, Bazzi R, Flores MA, Zheng W, Lebbou K, Tillement O, Mercier B, Dujardin C, Perriat P (2003) Synthesis and characterization of Gd_2O_3:Eu^{3+} phosphor nanoparticles by a sol-lyophilization technique. J Solid State Chem 173(2): 335–341

McDonald MA, Watkin KL (2006) Investigations into the physicochemical properties of dextran small particulate gadolinium oxide nanoparticles. Acad Radiol 13(4): 421–427

Mercier F, Alliot C, Bion L, Thromat N, Toulhoat P (2006) XPS study of Eu(III) coordination compounds: core levels binding energies in solid mixed-oxo-compounds $Eu_mX_xO_y$. J Electron Spectrosc Relat Phenom 150(1):21–26

Na HB, Hyeon T (2009) Nanostructured T1 MRI contrast agents. J Mater Chem 19(35):6267–6273

Nachimuthu P, Thevuthasan S, Engelhard MH, Weber WJ, Shuh DK, Hamdan NM, Mun BS, Adams EM, McCready DE, Shutthanandan V, Lindle DW, Balakrishnan G, Paul DM, Gullikson EM, Perera RCC, Lian J, Wang LM, Ewing RC (2004) Probing cation antisite disorder in $Gd_2Ti_2O_7$ pyrochlore by site-specific near-edge X-ray-absorption fine structure and X-ray photoelectron spectroscopy. Phys Rev B 70(10):100101

Nakamoto K (1997) Infrared and Raman spectra of inorganic and coordination compounds, 5th edn. John Wiley & Sons, New York

Norman P, Bishop DM, Jensen HJAa, Oddershede J (2001) Near-resonant absorption in the time-dependent self-consistent field and multiconfigurational self-consistent field approximations. J Chem Phys 115(22):10323

Norman P, Bishop DM, Jensen HJAa, Oddershede J (2005) Nonlinear response theory with relaxation: the first-order hyperpolarizability. J Chem Phys 123(19):194103

Ogasawara H, Kotani A (1995) Calculation of magnetic circular dichroism of rare-earth elements. J Phys Soc Jpn 64(4): 1394–1401

Park JY, Choi ES, Baek MJ, Lee GH, Woo S, Chang Y (2009) Water-soluble ultra small paramagnetic or superparamagnetic metal oxide nanoparticles for molecular MR imaging. Eur J Inorg Chem 17:2477–2481

Patil KC, Chandrashekhar GV, George MV, Rao CNR (1968) Infrared spectra and thermal decompositions of metal acetates and dicarboxylates. Can J Chem 46(2): 257–265

Peng XM, Huang MX, Gu L, Lin BL, Chen GH (2009) Characteristics of patients with liver disease intravenously exposed to diethylene glycol in China 2006. Clin Toxicol 47(2):124–131

Petoral RM Jr, Söderlind F, Klasson A, Suska A, Fortin MA, Abrikossova N, Selegård L, Käll P-O, Engström M, Uvdal K (2009) Synthesis and characterization of Tb^{3+}-doped Gd_2O_3 nanocrystals: a bifunctional material with combined fluorescent labeling and MRI contrast agent properties. J Phys Chem C 113(17):6913–6920

Plaschke M, Rothe J, Denecke MA, Fanghänel T (2004) Soft X-ray spectromicroscopy of humic acid europium(III) complexation by comparison to model substances. J Electron Spectrosc Relat Phenom 135(1):53–62

Rahman AATM, Vasilev K, Majewski P (2011) Ultra small Gd_2O_3 nanoparticles: absorption and emission properties. J Colloid Interface Sci 354(2):592–596

Raiser D, Deville JP (1991) Study of XPS photoemission of some gadolinium compounds. J Electron Spectrosc Relat Phenom 57:91–97

Rieter WJ, Taylor KML, An H, Lin W, Lin W (2006) Nanoscale metal–organic frameworks as potential multimodal contrast enhancing agents. J Am Chem Soc 128(28):9024–9025

Rowe MD, Chang C-C, Thamm DH, Kraft SL, Harmon JF, Vogt AP, Sumerlin BS, Boyes SG (2009a) Tuning the magnetic resonance imaging properties of positive contrast agent nanoparticles by surface modification with RAFT polymers. Langmuir 25(16):9487–9499

Rowe MD, Thamm DH, Kraft SL, Boyes SG (2009b) Polymer-modified gadolinium metal–organic framework nanoparticles used as multifunctional nanomedicines for the targeted imaging and treatment of cancer. Biomacromole cules 10(4):983–993

Schep LJ, Slaughter RJ, Temple WA, Beasley DMG (2009) Diethylene glycol poisoning. Clin Toxicol 47(6):525–535

Schwartz DA, Norberg NS, Nguyen QP, Parker JM, Gamelin DR (2003) Magnetic quantum dots: synthesis, spectroscopy, and magnetism of Co^{2+}- and Ni^{2+}-doped ZnO nanocrystals. J Am Chem Soc 125(43):13205–13218

Shu C, Corwin FD, Zhang J, Chen Z, Reid JE, Sun M, Xu W, Sim JH, Wang C, Fatouros PP, Esker AR, Gibson HW, Dorn HC (2009) Facile preparation of a new gadofullerene-based magnetic resonance imaging contrast agent with high 1H relaxivity. Bioconjug Chem 20(6):1186–1193

Skotland T, Iversen T-G, Sandvig K (2010) New metal-based nanoparticles for intravenous use: requirements for clinical success with focus on medical imaging. Nanomedicine NBM 6(6):730–737

Smith PH, Ryan RR (1992) Structure of a gadolinium hexaaza macrocycle complex with a $Gd_2(OAc)_8$ counterion. Acta Cryst C 48(12):2127–2130

Söderlind F, Pedersen H, Petoral RM Jr, Käll P-O, Uvdal K (2005) Synthesis and characterisation of Gd_2O_3 nanocrystals functionalised by organic acids. J Colloid Interface Sci 288(1):140–148

Stöhr J (1992) NEXAFS spectroscopy. Springer series in surface sciences, vol 25. Springer, New York

Takayama Y, Shinoda M, Obu K, Lee C, Shiozawa H, Hirose M, Ishii H, Miyahara T, Okamoto J (2002) Magnetic circular dichroism of X-ray emission for gadolinium in 4d–4f excitation region. J Phys Soc Jpn 71(1):340–346

Thole BT, van der Laan G, Fuggle JC, Sawatzky GA, Karnatak RC, Esteva JM (1985) 3d X-ray-absorption lines and the $3d^9 4f^{n+1}$ multiplets of the lanthanides. Phys Rev B 32(8):5107–5118

Toth E, Bolskar RD, Borel A, Gonzalez G, Helm L, Merbach AE, Sitharaman B, Wilson LJ (2005) Water-soluble gadofullerenes: toward high-relaxivity, pH-responsive MRI contrast agents. J Am Chem Soc 127(2):799–805

Urquhart SG, Ade H (2002) Trends in the carbonyl core (C 1s, O 1s) $\rightarrow \pi^*_{C=O}$ transition in the near-edge X-ray absorption fine structure spectra of organic molecules. J Phys Chem B 106(34):8531–8538

Vohs JM, Barteau MA (1988) Reaction pathways and intermediates in the decomposition of acetic and propionic acids on the polar surfaces of zinc oxide. Surf Sci 201(3):481–502

Watts JF, Wolstenholme J (2003) An introduction to surface analysis by XPS and AES. John Wiley & Sons Ltd, Chichester

Weller MT (1994) Inorganic materials chemistry. Oxford chemistry primers. Oxford University Press, Oxford

Yan B, Gu J, Xiao X (2010) $LnPO_4$:RE^{3+} (La = La, Gd; RE = Eu, Tb) nanocrystals: solvo-thermal synthesis, microstructure and photoluminescence. J Nanopart Res 12(6):2145–2152

Yanai T, Tew DP, Handy NC (2004) A new hybrid exchange-correlation functional using the Coulomb-attenuating method (CAM-B3LYP). Chem Phys Lett 393(1–3):51–57

Zhang MF, Liu JM, Liu ZG (2004) Microstructural characterization of nanosized $YMnO_3$ powders: the size effect. Appl Phys A 79(7):1753–1756

Zhang J, Fatouros PP, Shu C, Reid J, Owens LS, Cai T, Gibson HW, Long GL, Corwin FD, Chen Z-J, Dorn HC (2010a) High relaxivity trimetallic nitride (Gd_3N) metallofullerene MRI contrast agents with optimized functionality. Bioconjug Chem 21(4):610–615

Zhang X, Ballem MA, Ahrén M, Suska A, Bergman P, Uvdal K (2010b) Nanoscale Ln(III)-carboxylate coordination polymers (Ln = Gd, Eu, Yb): temperature-controlled guest encapsulation and light harvesting. J Am Chem Soc 132(30):10391–10397